Suplemento de la Revista Mexicana de Física **1** (2) 38–44 JUNE–JULY 2020

Liquid metal MHD steady flow and heat transfer in a rectangular duct with perfectly conducting walls perpendicular to the applied magnetic field

V. Solano-Olivares[a,*], S. Cuevas[a], and A. Figueroa[b]
[a] *Instituto de Energías Renovables, Universidad Nacional Autónoma de México, Apartado Postal 34, Temixco, Morelos 62580, México.*
**e-mail: vso@ier.unam.mx*
[b] *CONACYT-Centro de Investigación en Ciencias, Universidad Autónoma del Estado de Morelos, Cuernavaca, Morelos 62209, México.*

Received 18 February 2020; accepted 21 March 2020

Several technological applications involve the flow of liquid metals in ducts under a magnetic field, for instance, the coolants of fusion reactors. In this paper, using a magnetohydrodynamic MHD formulation based on the electric potential, we obtain an analytical solution for the flow of a liquid metal in a rectangular duct with two insulating walls and two perfectly conducting walls perpendicular to the applied uniform magnetic field. As the Hartmann number increases, the flow displays high velocities in the boundary layers attached to the insulating walls and a quasi-stagnant flow at the core. The effect of this flow pattern on the forced convection heat transfer is then explored numerically considering a uniform heat flux on either the conducting or insulating walls. Compared to the hydrodynamic case, the MHD flow enhances the heat transfer as the Hartmann number increases only in the case when the heat flux is applied at the insulating walls where high velocities are present. The increase of the local Nusselt number as the Péclet number grows indicates an efficient heat removal from the heated wall.

Keywords: Heat transfer; liquid metal MHD flow; analytical solution; perfectly conducting Hartmann walls; Nusselt number.

PACS: 47.15.-x; 47.60.+i; 47.65.-d

1. Introduction

Liquid metal magnetohydrodynamic (MHD) duct flows are relevant in different technological applications such as MHD generators, electromagnetic pumps, metallurgical processes [1] and, particularly, the design of fusion reactor blankets [2]. Since the experimental study of this kind of flow is expensive and complex, a great effort has been devoted to the search of analytical solutions in restricted conditions as well as to the development of computing codes able to simulate more realistic situations. In fact, several exact solutions of MHD flows in ducts have been extensively used to validate numerical codes, see for instance [3–6]. MHD flow patterns are determined by the magnetic forces that arise in the conducting fluid owing to the interaction of the applied magnetic field with electric currents induced by the fluid motion within the same field. In turn, current paths (particularly the way they close) depend on the electrical conductivity not only of the liquid metal but also of the duct walls. Therefore, ducts with different configurations of walls of distinct conductivity may lead to very different flow patterns. Since the forced convection heat transfer depends strongly on the flow distribution, it is of relevance to explore MHD flows in ducts with diverse wall configurations. As a matter of fact, many cases have been treated in the literature (see for instance [7, 8]).

Pioneering works in this area include Hunt's contributions [9, 10] where fully developed incompressible flows in ducts with rectangular cross-section under a uniform magnetic field transverse to a pair of walls were analysed. In his first contribution [9], Hunt obtained an exact solution for a duct with perfectly conducting walls perpendicular to the applied field and thin conducting walls parallel to the field. In these conditions, the electric current distribution may lead to the formation of the so-called "M-shaped" or "M-type" velocity profiles which are important in the context of liquid metal blanket applications [11]. A key dimensionless parameter in MHD flows is the Hartmann number, Ha, (to be defined below) whose square can be interpreted as the ratio of magnetic to viscous forces [8]. Hunt's solution showed that at high Hartmann numbers, high velocities are found close to the walls parallel to the field while the core remains almost stagnant. This flow pattern is particularly interesting since the presence of high velocities near the walls may promote the appearance of instabilities [12] and eventually turbulence [13], with a direct effect on the heat transfer [14]. In fact, recently an analytical solution of the heat transfer problem for the Hunt's flow has been reported [16].

According to the choice of the flow and electromagnetic variables, different equivalent formulations of the MHD equations are available [15]. The most common ones are the B-formulation, based on the induced magnetic field vector, and the ϕ-formulation, based on the scalar electric potential. Less common formulations involve the use of the magnetic vector potential or the electric current density vector [15]. In fact, Hunt's exact solution [9] was found using the B-formulation. In this work, we obtain an exact solution for the MHD flow in a rectangular duct with two perfectly conducting walls perpendicular to the uniform magnetic field and two insulating walls parallel to the field. Although this solution is well known in terms of the B-formulation [7], apparently it has not been reported for the ϕ-formulation. Therefore, it could be useful for the validation of numerical codes based

on the latter. In order to assess the effect of the MHD flow in the heat transfer process, we use the velocity profile of the exact solution to solve numerically the three-dimensional heat transfer problem in which a pair of walls, either the conducting or the insulating ones, are exposed to a uniform heat flux.

In Sec. 2, we present the formulation of the problem. The analytical solution for the MHD flow is developed in Sec. 3, while numerical heat transfer results are presented in Sec. 4. Finally, some concluding remarks are exposed in Sec. 5.

2. Formulation

We consider the fully developed flow of a viscous, incompressible electrically conducting fluid in a duct of constant rectangular cross-section under a transverse uniform magnetic field. It is assumed that the applied field is perpendicular to a pair of perfectly conducting walls and is parallel to a pair of insulating walls. In addition, a constant and uniform heat flux is applied at both perfectly conducting walls, while the insulating walls parallel to the field remain adiabatic. Figure 1 shows a sketch of the treated problem. The case where the heat flux is applied to the insulating walls is also considered. We first obtain an analytical solution for the MHD flow which is used to solve the heat transfer problem numerically using the finite volume method. For this study the working fluid is supposed to be a liquid metal.

In liquid metal MHD flows at laboratory and industrial scales, the low magnetic Reynolds numbers approximation ($R_m \ll 1$) holds [8], which indicates that magnetic fields induced by the motion of the fluid are much smaller than the applied magnetic field. Under this approximation and using the ϕ-formulation, the governing MHD equations in dimensionless terms are expressed in the form [15]

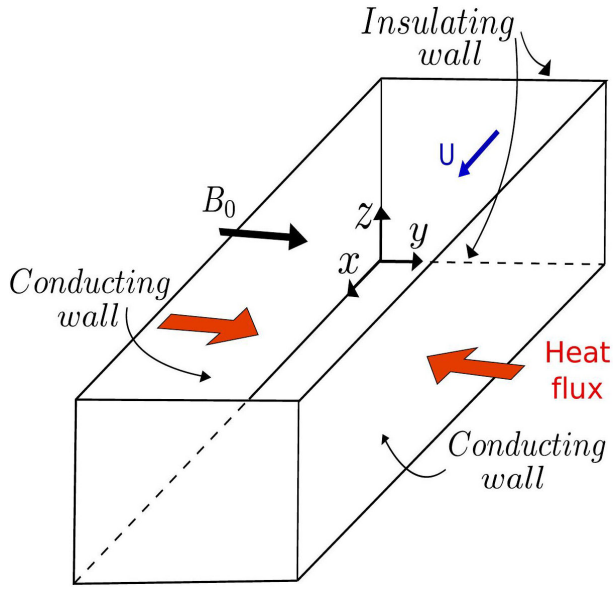

FIGURE 1. Sketch of flow and heat transfer of the analyzed problem.

$$\nabla \cdot \mathbf{u} = 0, \tag{1}$$

$$\frac{\partial \mathbf{u}}{\partial t} + (\mathbf{u} \cdot \nabla)\,\mathbf{u} = -\nabla P + \frac{1}{Re}\nabla^2 \mathbf{u} + N\mathbf{J} \times \mathbf{B}_0, \tag{2}$$

$$\mathbf{J} = -\nabla\phi + \mathbf{u} \times \mathbf{B}_0, \tag{3}$$

$$\nabla^2 \phi = \nabla \cdot (\mathbf{u} \times \mathbf{B}_0), \tag{4}$$

the velocity, $\mathbf{u}$, pressure, P, electrical current density, $\mathbf{J}$, applied magnetic field, $\mathbf{B}_0$, and electric potential, ϕ, are normalized by U, ρU^2, $\sigma U B_0$, B_0 and $L_c U B_0$, respectively, where the characteristic velocity, U, is the entrance flow velocity, B_0 is the characteristic magnetic field strength, ρ and σ are the mass density and electrical conductivity of the liquid, while L_c is the characteristic length which is taken as half the distance between the insulating walls. Coordinates (x,y,z) are normalized by L_c, and time t is normalized by inertial time L_c/U in the Navier-Stokes Eq. (2). The dimensionless control parameters are the Reynolds number, $Re = UL_c/\nu$, and the interaction parameter, $N = \sigma B_0^2 L_c/\rho U$, which is related to the Hartmann number since $N = Ha^2/Re$, where $Ha = B_0 L_c\,(\sigma/\rho\nu)^{1/2}$.

In addition, the applied magnetic field $\mathbf{B}_0$, must satisfy the magnetostatic equations, which guarantee its solenoidal and irrotational character, that is,

$$\nabla \cdot \mathbf{B}_0 = 0, \qquad \nabla \times \mathbf{B}_0 = 0. \tag{5}$$

The heat transfer equation for the liquid metal MHD flow is expressed in dimensionless form as

$$\frac{\partial T}{\partial t} + Pe\,(\mathbf{u} \cdot \nabla)\,T = \nabla^2 T, \tag{6}$$

where the temperature, T, has been normalized by the characteristic temperature T_0, which can be chosen as the inlet fluid temperature. In this equation, time t is normalized with the diffusive time L_c^2/α, where α is the thermal diffusivity of the liquid metal. The dimensionless control parameter is the Péclet number $Pe = UL_c/\alpha$, which can also be written as $Pe = PrRe$. Equation (6) does not consider the heat sources provided by viscous and Joule dissipations since compared to the inlet heat flux, they are usually negligible [14].

3. Analytical solution of the MHD flow

By considering a steady fully developed flow in the x-direction under a uniform magnetic field applied in the y-direction, the set of Eqs. (1)-(5) are reduced to

$$\frac{\partial^2 u}{\partial y^2} + \frac{\partial^2 u}{\partial z^2} + \frac{Ha^2}{k^2}\left(\frac{\partial \phi}{\partial z} - u\right) = \frac{1}{k}\frac{dP}{dx}, \tag{7}$$

$$\frac{\partial^2 \phi}{\partial y^2} + \frac{\partial^2 \phi}{\partial z^2} - \frac{\partial u}{\partial z} = 0, \tag{8}$$

where u is the velocity component in the x-direction and k is the duct's aspect ratio $k = y_0/z_0$, y_0 and z_0 being half the distance between the conducting and insulating walls,

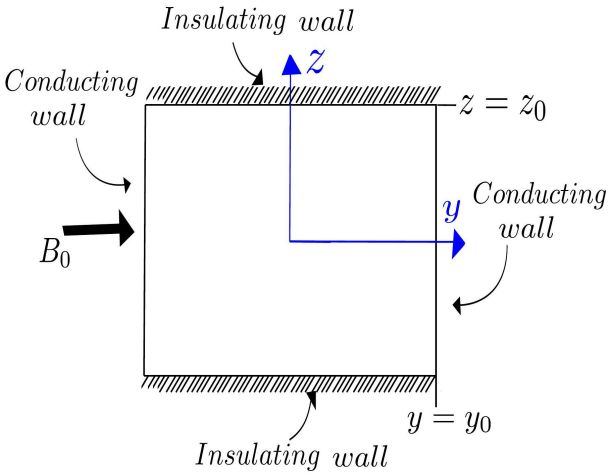

FIGURE 2. Sketch of the physical domain for the analytical solution.

respectively (see Fig. 2). The axial pressure gradient, dP/dx, is assumed to be constant, where the pressure was renormalized by $\rho\nu U/L_c$.

The velocity component u satisfies non-slip boundary conditions at all the duct walls. At the perfectly conducting walls, the electric field tangential to the walls must be zero while at the insulating walls the normal component of the current density has to be zero [7]. In terms of the electric potential, ϕ, the boundary conditions at the perfectly conducting and insulating walls are expressed, respectively, in the form

$$\frac{\partial\phi}{\partial z}(\pm y_0, z) = 0, \qquad \frac{\partial\phi}{\partial z}(y, \pm z_0) = 0. \tag{9}$$

The velocity field which satisfies the boundary conditions is given by

$$u(y,z) = \sum_{n=1,3\ldots}^{\infty}\sum_{m=1,3\ldots}^{\infty} A_{mn}\cos\frac{n\pi y}{2k}\sin\frac{m\pi z}{2}, \tag{10}$$

where

$$A_{mn} = \frac{-\frac{16}{k}\frac{dP}{dx}\left(m^2+\frac{n^2}{k^2}\right)\sin\frac{n\pi}{2}\cos\frac{m\pi}{2}}{mn\pi^2\left[\frac{\pi^2}{4}\left(m^2+\frac{n^2}{k^2}\right)^2 + Ha^2\left(\frac{n^2}{k^4}\right)\right]}. \tag{11}$$

In turn, the solution for the electric potential is expressed as

$$\phi(y,z) = \frac{2}{\pi}\sum_{n=1,3\ldots}^{\infty}\sum_{m=1,3\ldots}^{\infty} B_{mn}\cos\frac{n\pi y}{2k}\sin\frac{m\pi z}{2}, \tag{12}$$

where

$$B_{mn} = \frac{-\frac{16}{k}\frac{dP}{dx}\sin\frac{n\pi}{2}\cos\frac{m\pi}{2}}{n\pi^2\left[\frac{\pi^2}{4}\left(m^2+\frac{n^2}{k^2}\right)^2 + Ha^2\left(\frac{n^2}{k^4}\right)\right]}. \tag{13}$$

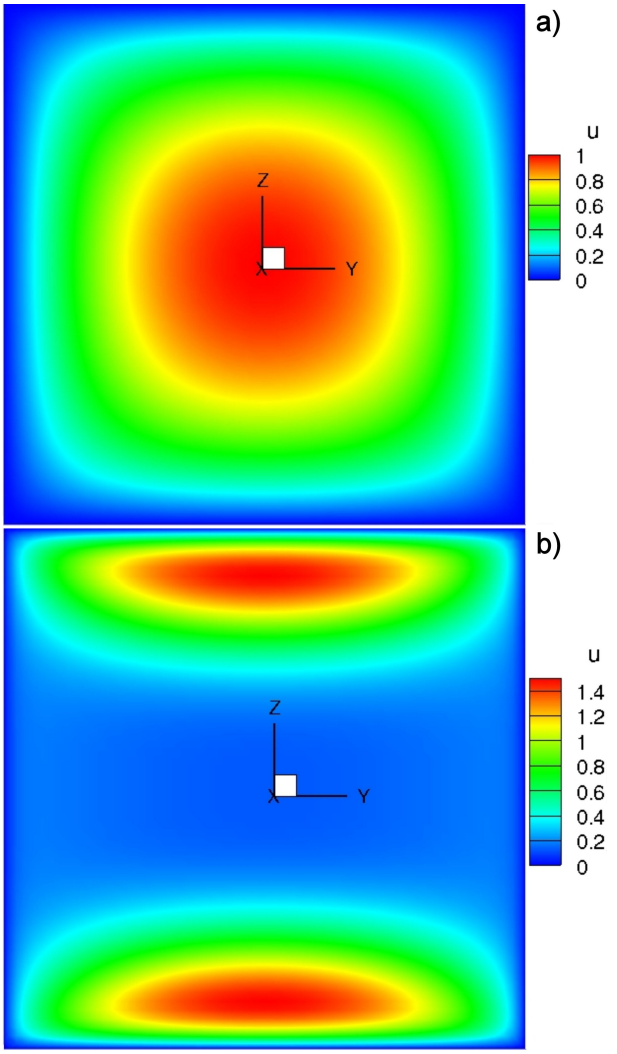

FIGURE 3. Magnitude of the velocity component in the flow domain (square duct, $k = 1$). a)$Ha = 0$ and b)$Ha = 30$.

Therefore, using Ohm's law, Eq. (3), the electrical current density field is given by

$$j_y = \frac{1}{k}\sum_{n=1,3\ldots}^{\infty}\sum_{m=1,3\ldots}^{\infty} nB_{mn}\sin\frac{n\pi y}{2k}\sin\frac{m\pi z}{2}, \tag{14}$$

$$j_z = \frac{1}{k^2}\sum_{n=1,3\ldots}^{\infty}\sum_{m=1,3\ldots}^{\infty} \frac{n^2}{m}B_{mn}\cos\frac{n\pi y}{2k}\cos\frac{m\pi z}{2}. \tag{15}$$

Although not shown here, it was verified that the present analytical solution has a perfect matching with the solution obtained with $B-$ formulation [7].

Figure 3 shows the magnitude of the velocity component for Hartmann numbers $Ha = 0$ and 30 for a square duct ($k = 1$). Evidently, $Ha = 0$ corresponds to the hydrodynamic flow which displays a parabolic profile with maximum velocity at the center. Likewise, for $Ha = 30$ the locations of the maximum velocity are displaced near both insulating walls. In fact, for high values of Ha, the flow exhibits a pair of jets close to the insulating walls while the core flow becomes almost stagnant.

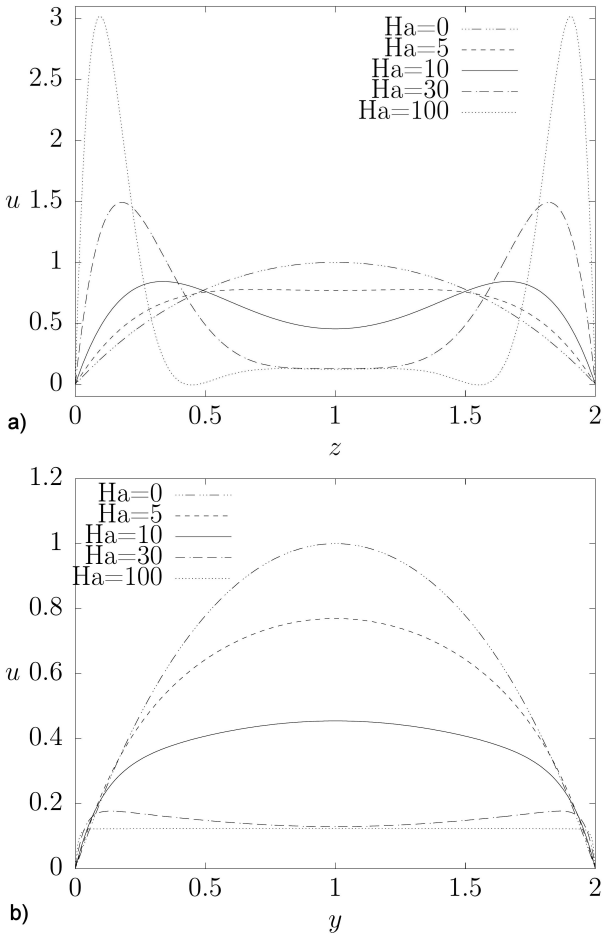

FIGURE 4. Velocity profiles in a square duct ($k = 1$) for different Ha values. a)Velocity as a function of z-coordinate, and b)Velocity as a function of y-coordinate.

This is clearly shown in Fig. 4a) where the velocity profiles as a function of z-coordinate are displayed for different Hartmann numbers ($Ha = 0, 5, 10, 30, 100$). The coordinate system was moved from the center of the duct to the lower-left corner to fit it with the system used in the heat transfer numerical code. Note that insulating walls are located at $z = 0$ and $z = 2$. On the other hand, Fig. 4b) shows the velocity profiles for the same Hartmann numbers but as a function of the y-coordinate. In this case, the effect of increasing the Hartmann number is to flatten the velocity profiles. As a result, mass flow is mainly carried by the side jets near the insulating walls, not by the bulk in the central region.

Figure 5a) shows isolines of electric potential while Fig. 5b) displays the corresponding electric current density vector field in the square duct for Ha=30. The analysis of the electric current distribution dictated by the conducting and insulating walls explains the flow pattern structure. As the Hartmann number increases, near the insulating walls the current density is almost parallel to the applied magnetic field and therefore, the braking Lorentz force $\mathbf{J}\times\mathbf{B}_0$ is negligible promoting the appearance of high-velocity regions. On the other hand, in the central region the current density is perpendicular to the applied magnetic field and the Lorentz force that brakes the flow is maximum causing the reduction of velocity in this region.

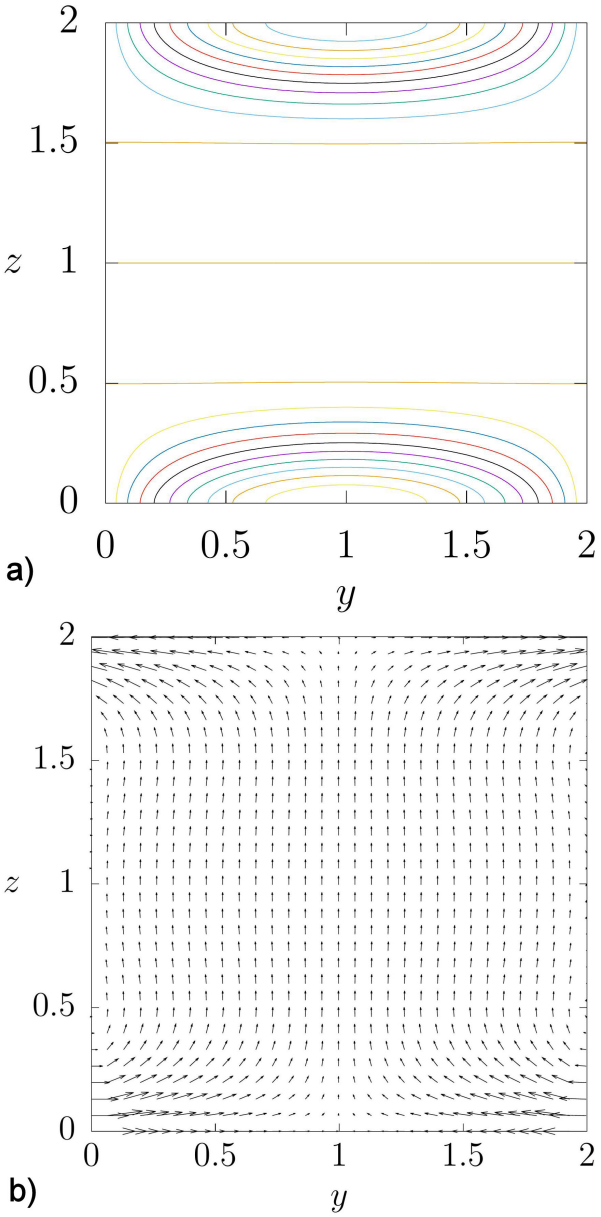

FIGURE 5. Electric potential and current density for $k = 1$, $Ha = 30$. a) Electric potential isolines, and b) Electric current density vector field.

4. Heat transfer numerical results

As it was mentioned above, the analytical velocity profile was used to solve the forced convection heat transfer problem in the duct, assuming that a pair of walls, either the perfectly conducting or the insulating ones, receive a constant uniform heat flux. We consider that the duct has a square cross-section whose dimensions in the $x-y-z$-directions are $10\times 2\times 2$, respectively, in dimensionless units. At the inlet, the fluid

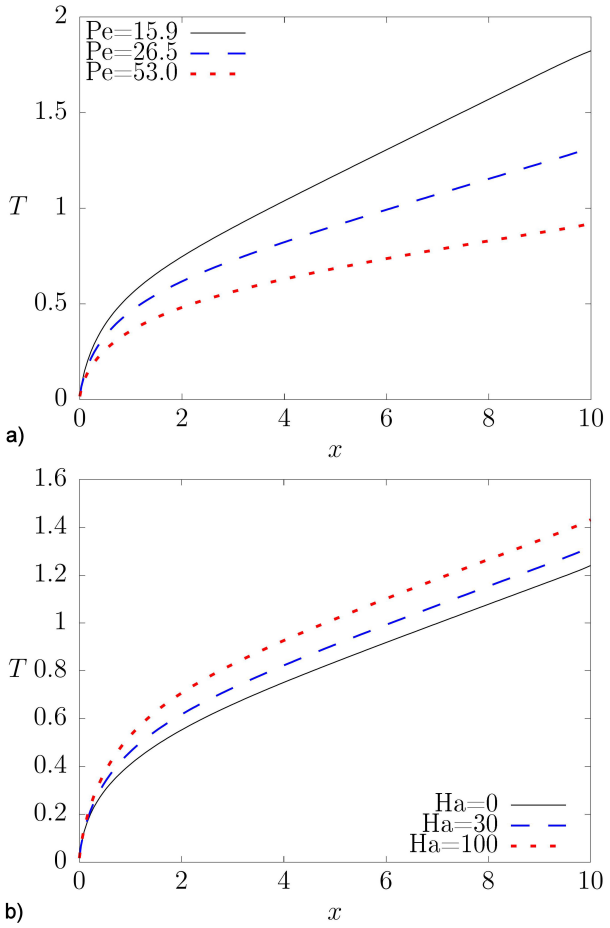

FIGURE 6. Temperature profiles at the heated perfectly conducting wall, $z = 1$, at $y = 0$, for different Péclet and Hartmann numbers ($k = 1$). a) $Ha = 30$, and b) $Pe = 26.5$.

temperature is assumed to be constant. Mathematically, the thermal boundary conditions applied to the solution of Eq. (6) for the case in which the heat flux enters at the perfectly conducting walls are:

$$\frac{\partial T}{\partial z} = 0, \quad z = 0, 2, \quad 0 \leq y \leq 2, \quad 0 \leq x \leq 10, \tag{16}$$

$$\frac{\partial T}{\partial y} = 1, \quad y = 0, 2, \quad 0 \leq z \leq 2, \quad 0 \leq x \leq 10, \tag{17}$$

$$T = 0, \quad x = 0, \quad 0 \leq y \leq 2, \quad 0 \leq z \leq 2, \tag{18}$$

The finite volume method (FVM) was used to solve the heat transfer equation [18] and the Euler method was used to discretize the temporal term. Derivatives were discretized using the finite difference approximation while the upwind differencing approach was used to calculate the convective term.

Figure 6a) shows the temperature profile in the mid plane $y = 0$ at the heated perfectly conducting wall, $z = 1$, as a function of x-coordinate for a Hartmann number $Ha = 30$ and different Péclet numbers, $Pe = 15.9, 26.5, 53$. It can be clearly observed that as the Péclet number grows, the wall temperature decreases, indicating a heat transfer enhancement. In turn, Fig. 6b) shows the temperature profiles at the heated (perfectly conducting) wall, $z = 1$, for three different Ha numbers $Ha = 0, 30, 100$ and a fixed Péclet number $Pe = 26.5$. It can be noticed that the lowest wall temperature is obtained when $Ha = 0$, that is, when the profile is the hydrodynamic one. As Ha increases, the wall temperature increases manifesting the influence of the small velocities found at the heated wall due to a stronger opposing Lorentz force. Therefore, in this case the hydrodynamic parabolic profile leads to a more efficient heat removal than the flat MHD profile (see Fig. 4b)).

Figure 7 shows the local Nusselt number at the heated perfectly conducting wall as a function of x-coordinate for different Péclet numbers, $Pe = 53, 530, 2650$, and a fixed Hartmann number $Ha = 30$. The local Nusselt number, also known as the local heat transfer coefficient, is defined as

$$Nu_x(x,t) = \left.\frac{\partial T}{\partial y}\right|_w \frac{L_y}{T_b - T_w}, \tag{19}$$

where L_y is the distance between the heated walls, T_w is the wall temperature and T_b is the bulk temperature given by

$$T_b(x,t) = \frac{\int_0^{L_y} uT dy}{\int_0^{L_y} u dy}. \tag{20}$$

The parameter Nu_x gives information about the local heat transfer rate and, as it is expected, the larger the Péclet number, the larger the heat removal and the lower the wall temperature, as discussed in Fig. 6a).

Let us now explore the heat transfer when the uniform heat flux is applied at the insulating walls. An effect is expected since the flow exhibits high velocity jets near the insulating walls, parallel to the applied magnetic field. Figure 8 shows the wall temperature profiles along a heated insulating wall, $y = 1$, at the mid plane $z = 0$, as a function of the x-coordinate for the same parameters used in Fig. 6. As in the previous case (see Fig. 6a)), Fig. 8a) shows that the larger the the Péclet number for a given Hartmann number ($Ha = 30$)

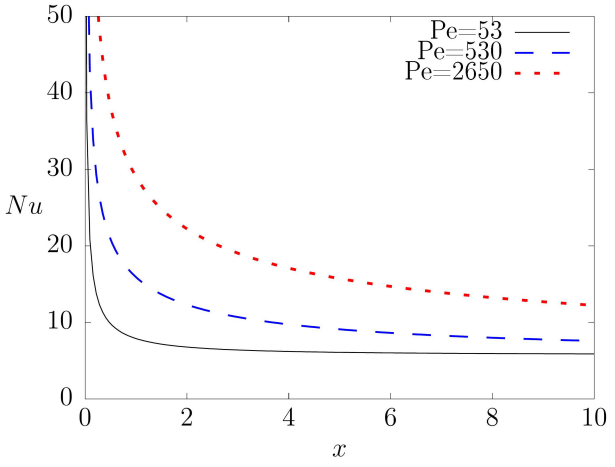

FIGURE 7. Local Nusselt number as a function of x coordinate for different Péclet numbers when $Ha = 30$.

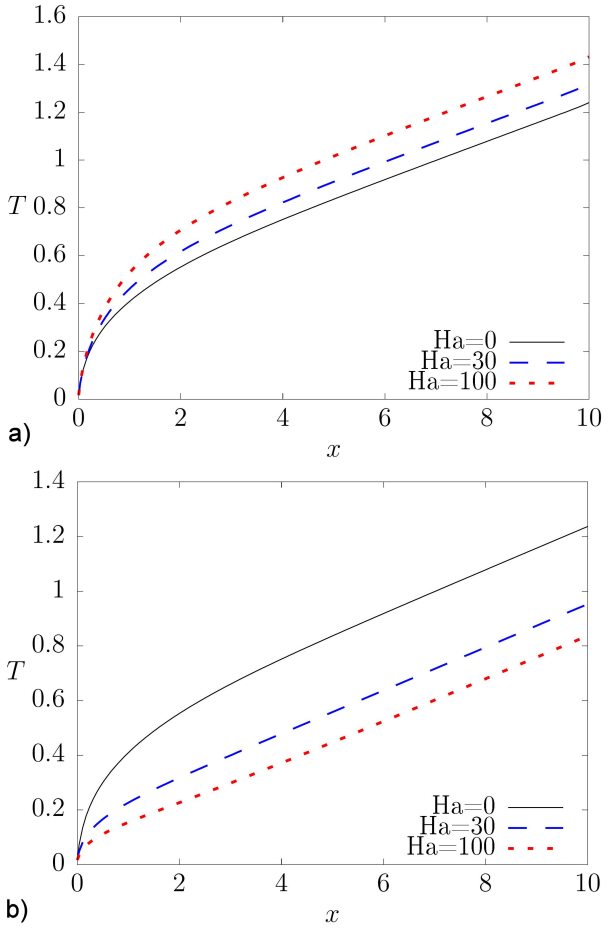

FIGURE 8. Temperature profile at the heated insulating wall, $y = 1$, at $z = 0$ for different Péclet and Hartmann numbers ($k = 1$). a) $Ha = 30$, and b) $Pe = 26.5$.

the lower the wall temperature. However, in this case, the reduction in wall temperature is higher than the case of the heated conducting wall. In addition, Fig. 8b) shows the temperature profiles at the heated insulating wall for different Hartmann numbers observing that the higher the Hartmann number the lower the wall temperature. Evidently, this occurs due to the presence of the high-velocity jets that appear near these walls for high Ha promoting a more efficient heat removal.

5. Conclusion

In this paper, we used the MHD formulation based on the electric potential to obtain an exact analytical solution for the fully developed flow of a liquid metal in a duct of rectangular cross-section with two insulating walls and two perfectly conducting walls perpendicular to the applied magnetic field. This solution is equivalent to the reported solution in terms of the induced magnetic field [7]. The analytical velocity profile was used to explore numerically the forced convective heat transfer when a constant and uniform heat flux is imposed on either the perfectly conducting or the insulating walls. As expected, the heat transfer process is strongly influenced by the flow pattern which displays high-velocity regions near both insulating walls for high values of the Hartmann number. For a fixed Péclet number, when the heat flux enters the perfectly conducting walls, the hydrodynamic profile leads to a stronger heat removal and lower wall temperatures than the MHD profiles. However, when the surface heat flux is set at the insulating walls where the high velocity regions are formed, the heat removal is more efficient the larger the Hartmann number leading to lower wall temperatures. It was also verified that for a constant Hartmann number, the local Nusselt number increases as the Péclet number grows, which indicates a better heat removal from the heated wall.

Acknowledgments

A. F. thanks the Cátedras program and project 258623 both from CONACyT.

1. P. A. Davidson, Magnetohydrodynamics in materials processing. *Ann. Rev. Fluid Mech.* **31** (1999) 273. https://doi.org/10.1146/annurev.fluid.31.1.273
2. L. Bühler, Liquid metal magnetohydrodynamics for fusion blankets. *Magnetohydrodynamics* (2007) 171-194.
3. M. J. Ni, R. Munipalli, N. B. Morley, P. Huang, and M. A. Abdou, (2007). Validation case results for 2D and 3D MHD simulations. *Fusion Sci. Tech.* **52** 587. https://doi.org/10.13182/FST07-A1552
4. T. Zhou, Z. Yang, M. Ni, and H. Chen, Code development and validation for analyzing liquid metal MHD flow in rectangular ducts. *Fusion Eng. Design*, **85** (2010) 1736. https://doi.org/10.1016/j.fusengdes.2010.05.034
5. J. Mao, and H. Pan, Three-dimensional numerical simulation for magnetohydrodynamic duct flows in a staggered grid system. *Fusion Eng. Design* **88** (2013) 145. https://doi.org/10.1016/j.fusengdes.2013.01.092
6. S. Sahu, and R. Bhattacharyay, Validation of COMSOL code for analyzing liquid metal magnetohydrodynamic flow. *Fusion Eng. Design*, **127** (2018)151. https://doi.org/10.1016/j.fusengdes.2018.01.009
7. W. F. Hughes, and F. J. Young, *The electromagnetodynamics of fluids*. (New York: Wiley, 1966).
8. Müller, and L. Bühler, *Magnetofuiddynamics in channels and containers*. (Springer, Berlin, 2001).
9. J. C. R. Hunt, Magnetohydrodynamic flow in rectangular ducts. *J. Fluid Mech.*, **21** (1965) 577. https://doi.org/10.1017/S0022112065000344
10. J. C. R. Hunt, and K. Stewartson, Magnetohydrodynamic flow

in rectangular ducts II. *J. Fluid Mech.* **23** (1965) 563. https://doi.org/10.1017/S0022112065001544

11. S. Smolentsev, N. Vetcha, and M. Abdou, Effect of a magnetic field on stability and transitions in liquid breeder flows in a blanket. *Fusion Eng. Design* **88** (2013) 607. https://doi.org/10.1016/j.fusengdes.2013.04.001

12. T. Arlt, J. Priede, and L. Bühler, The effect of finite-conductivity Hartmann walls on the linear stability of Hunt's flow. *J. Fluid Mech.* **822** (2017) 880. https://doi.org/10.1017/jfm.2017.322

13. S. Cuevas, B. F. Picologlou, J. S. Walker, and G. Talmage, Liquid-metal MHD flow in rectangular ducts with thin conducting or insulating walls: laminar and turbulent solutions. *Int. J. Eng. Sci.*, **35** (1997) 485. https://doi.org/10.1016/S0020-7225(96)00126-7

14. S. Cuevas, B. F. Picologlou, J. S. Walker, G. Talmage, and T. Hua, Heat transfer in laminar and turbulent liquid-metal MHD flows in square ducts with thin conducting or insulating walls. *Int. J. Eng. Sci.* **35** (1997) 505. https://doi.org/10.1016/S0020-7225(96)00127-9

15. S. Smolentsev, S. Cuevas, and A. Beltrán, Induced electric current-based formulation in computations of low magnetic Reynolds number magnetohydrodynamic flows. *J. Comput. Phys* **229** (2010) 1558. https://doi.org/10.1016/j.jcp.2009.10.044

16. M. J. Bluck, and M. J. Wolfendale, An analytical solution to the heat transfer problem in thick-walled Hunt flow. *Int. J. Heat Fluid Flow* **64** (2017) 103. https://doi.org/10.1016/j.ijheatfluidflow.2017.03.002

17. Z. Li, J. Li, X. Li, and M. J. Ni, Free surface flow and heat transfer characteristics of liquid metal Galinstan at low flow velocity. *Exp. Thermal and Fluid Sci.* **82** (2017) 240-248. https://doi.org/10.1016/j.expthermflusci.2016.11.021

18. H. K. Versteg, and W. Malalasekera, *An introduction to computational fluid dynamics*. The finite volume method, (Longman, New York 1995).